Journal of Molecular Spectroscopy 276–277 (2012) 22–32

Contents lists available at SciVerse ScienceDirect

Journal of Molecular Spectroscopy

journal homepage: www.elsevier.com/locate/jms

Coriolis analysis of several high-resolution infrared bands of bicyclo[1 1 1]pentane-d_0 and -d_1 ☆

A. Perry [a], M.A. Martin [a], J.W. Nibler [a,*], A. Maki [b], A. Weber [c], T.A. Blake [d]

[a] Department of Chemistry, Oregon State University, Corvallis, OR 97332-4003, United States
[b] 15012 24th Avenue, S.E., Mill Creek, WA 98012, United States
[c] Sensor Science Division, National Institute of Standards and Technology, Gaithersburg, MD 20899, United States
[d] Pacific Northwest National Laboratory, P.O. Box 999, Mail Stop K8-88 Richland, WA 99352, United States

ARTICLE INFO

Article history:
Received 29 April 2012
In revised form 6 June 2012
Available online 16 June 2012

Keywords:
Bicyclopentane
High-resolution infrared spectrum
Rovibrational constants
Coriolis interactions
Ground state structure
DFT calculations
Anharmonic frequencies

ABSTRACT

High-resolution infrared absorption spectra have been analyzed for two bicyclo[1 1 1]pentane isotopologues, C_5H_8 (-d_0) and C_5H_7D (-d_1), where in the latter the D-atom replaces a hydrogen on the C_3 symmetry axis such that the molecular symmetry is reduced from D_{3h} to C_{3v}. Two (a_2'') parallel bands, ν_{17} and ν_{18}, of bicyclopentane-d_0 were studied and the former was found to be profoundly affected by Coriolis coupling with the nearby (e') perpendicular band, ν_{11}. Weaker coupling was observed between the ν_{18} band and the nearby $\nu_{13}(e')$ band, for which fewer transitions could be assigned. For bicyclopentane-d_1, the ν_5 parallel band was also studied along with the nearby $\nu_{15}(e')$ band to which it is coupled through a similar type of Coriolis resonance. For both isotopologues, quantum calculations (B3LYP/cc-pVTZ) done at the anharmonic level were very helpful in unraveling the complexities caused by the Coriolis interactions, provided that care is taken in identifying the effect of any Coriolis resonances on the theoretical values of α_B and q rovibrational parameters. The ground state B_0 constants were found to be 0.2399412(2) and 0.2267506(11) cm^{-1} for the -d_0 and -d_1 isotopologues. The difference yields an R_s substitution value of 2.0309(2) Å for the position of the axial H atom relative to the -d_0 center of mass, a result in good accord with a corresponding R_a value of 2.044(6) Å from electron diffraction data. For both isotopologues, the theoretical results from the quantum calculations are in good agreement with all corresponding values determined from the spectra.

1. Introduction

Our previous work on bicyclo[1 1 1]pentane (C_5H_8) was devoted to the determination of the ground state constants of this molecule from measurements on three different fundamental vibrations, $\nu_{14}(e')$ at 540 cm^{-1}, $\nu_{17}(a_2'')$ at 1220 cm^{-1}, and $\nu_{18}(a_2'')$ at 832 cm^{-1}, as well as some transitions from a partially analyzed $\nu_{11}(e')$ band at 1232 cm^{-1}. [1] In the course of this work it was found that the upper state levels of the ν_{14} band are unperturbed but the $\nu_{17}(a_2'')$ and $\nu_{18}(a_2'')$ bands showed evidence of strong and weak Coriolis interactions with nearby levels of the $\nu_{11}(e')$ and $\nu_{13}(e')$ fundamentals, respectively. The present work deals with these Coriolis interactions in order to not only determine the constants of the upper states of the $\nu_{17}(a_2'')$ and $\nu_{18}(a_2'')$ bands but also to deduce rovibrational parameters for the less intense ν_{11} and $\nu_{13}(e')$ bands.

In addition, the mono-deuterated isotopologue (C_5H_7D) of bicyclopentane was synthesized (with the D atom on the C_3 symmetry axis) and its infrared spectrum recorded at a resolution of 0.002 cm^{-1} to provide additional information on the properties of the bicyclopentane species. (Henceforth for brevity we will omit the specifier [1 1 1] and use bicyclopentane-d_0 and bicyclopentane-d_1 (or -d_0 and -d_1) to designate the normal (C_5H_8) and deuterated (C_5H_7D) species, respectively.) This work on bicyclopentane is an outgrowth of our earlier work on [1 1 1]propellane [2–4] and provides experimental data to better understand the bonding and molecular properties of these small ring-strained molecules. All three molecules are symmetric tops and their structures are shown in Fig. 1.

This work has benefitted from earlier investigations of the vibrational infrared and Raman spectra of bicyclopentane-d_0, -d_1, and -d_2 reported by the Wiberg group [5,6]. Although done at relatively low resolution, infrared spectra obtained at 0.06 cm^{-1} resolution did show some unresolved *J*, *K* rotational structure, from which approximate upper and ground state *B*-values were obtained for the ν_{17} and ν_{18} modes of bicyclopentane-d_0 and -d_2 [6]. The current 30-fold improvement in spectral resolution gives a much more complete view of the individual *J*, *K* lines, hence this

☆ Based in part on an undergraduate honors thesis of M. Martin, University Honors College, Oregon State University.

* Corresponding author. Fax: +1 541 737 2062.
E-mail addresses: niblerj@orst.edu, niblerj@chem.orst.edu (J.W. Nibler).

0022-2852/$ - see front matter © 2012 Elsevier Inc. All rights reserved.
http://dx.doi.org/10.1016/j.jms.2012.06.008

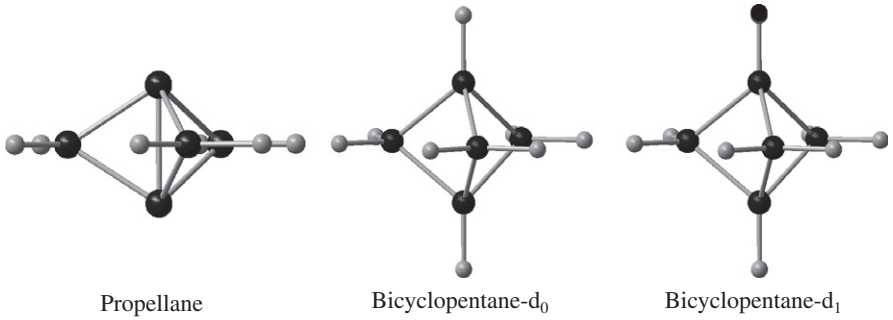

Fig. 1. Structural arrangements for [1 1 1]propellane, bicyclo[1 1 1]pentane-d_0, and bicyclo[1 1 1]pentane-d_1. The first two structures possess the symmetry of the point group D_{3h}, while the symmetry of the -d_1 isotopologue is C_{3v}.

Table 1
Frequencies and intensities of the fundamental modes of bicyclopentane-d_0.

Experiment[a]			Theory[b]			
					Relative intensity	
Mode			Harmonic	Anharmonic	Raman	IR
a_1'	1	2976	3092	***2950***	436 vs	…
	2	2887	3042	***2906***	370 s	…
	3	1509	1554	***1500***	5.2 vw	…
	4	1107	1119	1095	36 vs	…
	5	898	908	888	6.6 s	…
a_2'	6	–	3095	2952	…	…
	7	–	969	954	…	…
e'	8	2976	3100	2956	131 vs	72 vs
	9	2887	3037	***2888***	1.3 s	83 vs
	10	1456	1504	***1492***	5.3 vw	0.4 m
	11	**1231.41**	1259	1226	6.3 w	1.9 w
	12	1098	1117	1093	0.9	0.3 w
	13	**886.5**	898	874	4.3	0.4 w
	14	**540.34**	542	537	0.3 w	0.2 w
a_1''	15	–	1004	975	…	…
a_2''	16	2976	3087	2952	…	138 vs
	17	**1219.89**	1252	1221	…	37 s
	18	**832.93**	844	825	…	3.8 m
e''	19	–	1216	1186	0.2	…
	20	–	1144	1112	1.7	…
	21	1006	1029	1005	18 m	…
	22	769	774	747	5.9 m	…

[a] Ref [6], Table (VII). Values in boldface are from reference 1 and from this study.
[b] This work, B3LYP/cc-pVTZ calculations using Gaussian 09 with Anharm/Vibrot options. Anharmonic frequencies in bold italics are obtained from Gaussian and include correction for Fermi resonance. The qualitative experimental intensities (vw, w, m, s, vs), where available, are taken from Ref. [5].

Table 2
Frequencies and intensities of the fundamental modes of bicyclopentane-d_1.

Experiment[a]			Theory[b]			
					Relative intensity	
Mode			Harmonic	Anharmonic	Raman	IR
a_1	1	2975	3090	2952	232 vs	65 vs
	2	2886	3045	***2905***	384 s	4.0 s
	3	2223	2281	***2201***	92 s	39 s
	4	1501	1552	1498	6.0vw	0.0
	5	**1217.33**	1250	1218	0.1	36 s
	6	1086	1099	1077	38 vs	0.0 w
	7	892	905	886	5.4 m	0.0
	8	823	834	815	0.0	3.9 m
a_2	9	–	3095	2951	…	…
	10	–	1004	975	…	…
	11	–	969	954	…	…
e	12	2975	3100	2956	131 vs	72 vs
	13	2886	3037	***2888***	1.3 s	83 s
	14	1456	1504	***1490***	5.3 m	0.4 m
	15	**1210.31**	1238	1206	4.0 m	1.2
	16	1144	1171	1142	3.3 m	0.5 m
	17	1104	1142	1110	3.1 m	0.0
	18	–	1105	1079	5.3	0.1
	19	955	967	941	10 s	0.1 w
	20	798	808	784	1.3 w	0.2
	21	–	721	705	7.4	0.2
	22	538	540	535	0.3 w	0.2 w

[a] Ref [6], Table (VII). Values in boldface are from this study.
[b] This work, B3LYP/cc-pVTZ calculations using Gaussian 09 with Anharm/Vibrot options. Anharmonic frequencies in bold italics are obtained from Gaussian and include correction for Fermi resonance. The qualitative experimental intensities (vw, w, m, s, vs), where available, are taken from Ref. [5].

reinvestigation was done in order to obtain accurate values for the various constants that characterize the intra-molecular properties. We here account for the Coriolis perturbations that afflict the upper state levels of the ν_{17} and ν_{18} transitions as well as their counterparts (ν_5, ν_{15}) in bicyclopentane-d_1. The mode numbering for the fundamentals of bicyclopentane-d_0 and bicyclopentane-d_1 is given in Tables 1 and 2, along with wavenumber and approximate intensity values reported by Wiberg et al. [6]. Also given in the Tables are the corresponding values we have calculated in the anharmonic approximation using the Gaussian 09W program (method B3LYP, basis cc-pVTZ, options Anharm/Vibrot) [7].

2. Experimental

2.1. Synthesis

The synthesis of bicyclopentane-d_0 was described in [1] and was modified slightly for the synthesis of bicyclopentane-d_1. In both cases, the propellane precursor, prepared using the method reported by Mondanaro and Dailey [8], was reacted with a slight excess of thiophenol (HSPh) to produce phenyl bicyclopentyl sulfide.

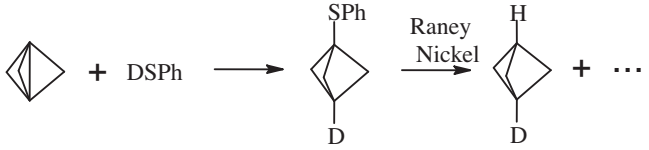

For the -d_1 synthesis, shown above, the thiophenol was deuterated at the sulfur position by three exchanges with D_2O (99.8%), yielding DSPh with a deuteration level estimated from NMR spectra to be in excess of 75%. Subsequent reaction with propellane yielded the mono-deuterated phenyl bicyclopentyl sulfide with the deuterium and the phenyl sulfide group in the axial positions.

After subsequent aqueous workup and treatment with Raney nickel as outlined in [1], the volatile products were collected at

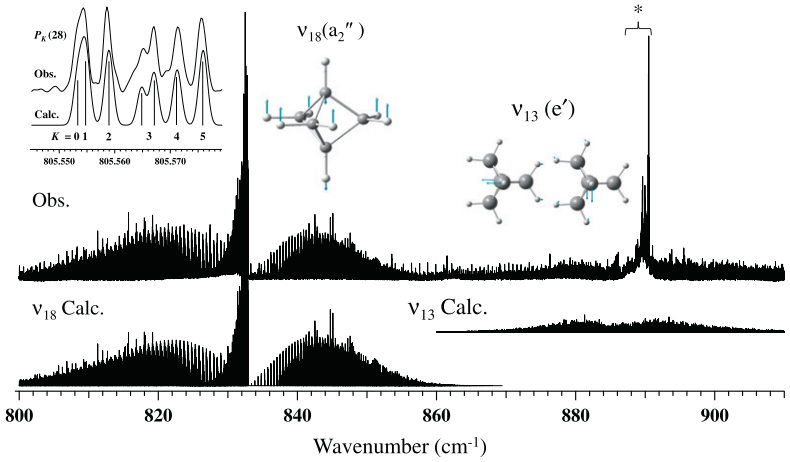

Fig. 2. Overview of the parallel (a_2'') ν_{18} and perpendicular (e') ν_{13} bands of bicyclopentane-d_0. The strong features labeled with an asterisk are attributed to 2-methyl-1-butene impurity in the sample. The inset show an expanded view of the K structure of the $P_K(28)$ feature in which the splitting of the $K = 3$ line is apparent.

77 K after passage through a trap at −78 °C to remove H_2O. The Raney nickel hydrogenation reaction is effective at breaking sulfur bonds to position a hydrogen atom at the apical position but also appears to break some of C–C ring bonds as well. An infrared spectrum of the mixture showed nearly equal amounts of d_0 and d_1 isotopologues but also significant amounts of benzene and isopentane, as had been reported in [1]. In addition a medium intensity absorption was observed at 891 cm^{-1} that is attributed to 2-methyl-1-butene and several Q-branch features due to allene were found. All of these hydrocarbon impurities are reasonable byproducts of the hydrogenation reaction and most are difficult to separate from bicyclopentane because they have comparable vapor pressures. Because of their presence and because of the low yield of bicyclopentane-d_1, for this isotopologue only the intense 1215 cm^{-1} ν_5 band region was judged suitable for analysis. Even in this case the analysis was complicated by some overlap with the corresponding bands in bicyclopentane-d_0 and also by Coriolis coupling to the nearby ν_{15} band. Despite this, it was possible to deduce accurate values for the ground state rotational constants for the -d_1 isotopologue, along with rovibrational constants for the upper states of its ν_5 and ν_{15} transitions.

2.2. Spectroscopy

High-resolution infrared spectra were recorded with the Bruker 125 Fourier transform spectrometer located at the Pacific Northwest National laboratory.[1] A Globar source and a mercury–cadmium–telluride detector were used. A White-type multiple reflection absorption cell adjusted for an absorption path length of 25.6 m was filled with the vapor of bicyclopentane-d_0 to a pressure of 143 Pascal (1.07 torr) to record the weak $\nu_{18}(a_2'')$ and $\nu_{13}(e')$ bands near 850 cm^{-1}. A total of 448 scans were averaged and, with Boxcar apodization, the instrumental resolution was 0.0015 cm^{-1}. For the more intense $\nu_{17}(a_2'')$ and $\nu_{11}(e')$ bands near 1250 cm^{-1}, a 20.0 cm cell filled to 1330 Pascal (9.98 torr) was used and 512 scans were averaged at resolution 0.002 cm^{-1}. In the case of bicyclopentane-d_1, only the region near 1225 cm^{-1} gave useful spectra and for this, 256 scans were averaged for a path length of of 12.8 m for the White cell which was filled to a total cell pressure of 72 Pascal (0.54 torr). The resolution was 0.002 cm^{-1}.

[1] Certain commercial equipment, instruments, and materials are identified in the paper to adequately specify the experimental procedure. Such identification does not imply recommendations or endorsements by the National Institute of Standards and Technology or the Pacific Northwest National Laboratory, nor does it imply that the materials or equipment identified are necessarily the best available for the purpose.

Spectral calibration was accomplished with N_2O and OCS using frequencies taken from the NIST compilations [9]. The corrections were less than 0.00015 cm^{-1} and the absolute wavenumber uncertainty is estimated to be ±0.00015 cm^{-1}. Figs. 2 and 3 give overviews of the -d_0 bands examined in this work, along with representations of the relevant normal modes. The details of the spectral analyses and expanded views of selected regions of the spectra will be given in the subsequent discussion.

3. Band analysis

The analysis of the bands proceeded in a standard manner for oblate symmetric top molecules. The energy of a given vibrational state v is given by

$$E_v = G(v,l) + F_v(J,K,l), \tag{1}$$

where $G(v, l)$ is the vibrational term, and the rotational term for non-degenerate vibrational states, $F_v(J, K)$, is given by

$$\begin{aligned} F_v(J,K) = {} & B_v J(J+1) + (C_v - B_v)K^2 - D_v^J J^2(J+1)^2 - D_v^{JK} J(J+1)K^2 \\ & - D_v^K K^4 + H_v^J J^3(J+1)^3 + H_v^{JK} J^2(J+1)^2 K^2 \\ & + H_v^{KJ} J(J+1)K^4 + H_v^K K^6 \pm \delta_{3K}\Delta_3 J(J+1)[J(J+1) \\ & - 2][J(J+1) - 6] + \cdots. \end{aligned} \tag{2}$$

For doubly degenerate vibrational states the rotational term expression is given by

$$F_v(J,K,l) = F_v(J,K) + F_{v\perp}(J,k,l), \tag{3}$$

in which

$$F_{v\perp}(J,k,l) = -2(C\zeta)_v kl + \eta_v^J J(J+1)kl + \eta_v^K k^3 l. \tag{4}$$

In these expressions J is the total angular momentum quantum number, k is the signed quantum number for the projection of the vector **J** onto the symmetry axis, $K = |k|$, and l is the vibrational angular momentum quantum number. The $(C\zeta)_v$ term in Eq. (4) accounts for the intra-vibrational Coriolis interactions; when the product kl is positive (negative) the vibrational and rotational angular momenta are parallel (antiparallel). The contracted subscript v is used to represent both quantum number and mode number of a vibrational state. For the ground state $v_1 = v_2 = v_3 = \cdots = 0$. The zero energy is defined as the $J = K = 0$ level of the ground state, i.e., $v_0 = G(v,l) - G(0,0)$.

In addition to the above, an off-diagonal l-type resonance term is included that has the primary effect of splitting the $kl = 1$ levels of a degenerate vibrational state with $l = \pm 1$. This term is defined as

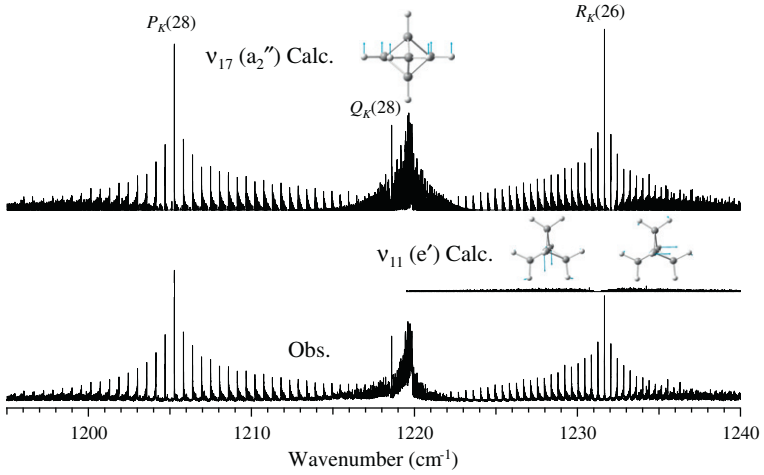

Fig. 3. Overview of the parallel (a_2'') ν_{17} and perpendicular (e') ν_{11} bands of bicyclopentane-d_0.

$$\begin{aligned} W_{2,2} &= \langle v,J,k,l|H|v,J,k\pm2,l\pm2\rangle \\ &= 1/4\{q+q_JJ(J+1)+q_k[k^2+(k\pm2)^2]\}\ [(v+1)^2 \\ &\quad -(l\pm1)^2]^{1/2}[J(J+1)-k(k\pm1)]^{1/2}[J(J+1) \\ &\quad -(k\pm1)(k\pm2)]^{1/2}, \end{aligned} \tag{5}$$

where H is the Hamiltonian operator of the interaction. This term also pushes apart other pairs of levels for which $\Delta k = \Delta l = \pm2$ but, since these levels are nondegenerate and are already separated by other terms, the effect is minimal compared with that on the otherwise degenerate $kl = 1$ levels. Sometimes the fits are improved by addition of the q_J and q_k terms which represent the effect of the centrifugal distortion, as do the D, H, and η parameters in Eqs. (2) and (4).

Finally, the effect of a Coriolis interaction between states whose product symmetry is that of a rotation (Jahn's rule) can have a profound effect on the spectra. Such an interaction is expected for each a_2'' and e' pair of modes considered here since the e'' product symmetry corresponds to the symmetry of the R_x, R_y rotations. As detailed in Refs. [10,11], this interaction can be described by an off-diagonal term which, in the case of the $\nu_{17}(a_2'')$ and $\nu_{11}(e')$ modes of bicyclopentane-d_0, can be written

$$\begin{aligned} W_{1,1} &= < v_{17}, v_{11}, J, k\pm1, l_{11}\pm1|H|v_{17}+1, v_{11}-1, J, k, l_{11}> \\ &= \pm2^{1/2}\Omega_{17,11}B\zeta^{y}_{17,11t2}[J(J+1)-k(k\pm1)]^{1/2} \\ &\quad + \text{higher terms} \\ &= \pm\{w_{1,1}+w_{1,1,J}J(J+1)+w_{1,1,k}[k^2+(k\pm1)^2]+w_{1,1,kl}[kl \\ &\quad +(k\pm1)(l\pm1)]\}[J(J+1)-k(k\pm1)]^{1/2}, \end{aligned} \tag{6}$$

where $\Omega_{17,11} = \frac{1}{2}[(\omega_{11}/\omega_{17})^{1/2}+(\omega_{17}/\omega_{11})^{1/2}] \approx \frac{1}{2}[(\nu_{11}/\nu_{17})^{1/2}+(\nu_{17}/\nu_{11})^{1/2}]$ is very close to 1 and is subsumed in the fitted parameter $w_{1,1}$. In calculating $w_{1,1}$ from theoretical results, we have used harmonic ω values, $B \approx B_e$ and $\zeta^{y}_{17,11t2}$, where the t_2 subscript refers to the degenerate component of ν_{11} that is antisymmetric with respect to reflection through a y–z plane. We note that, when the y axis contains one of the ring C atoms, the degenerate coordinates naturally have the appropriate symmetry and $\zeta^{y}_{17,11t1} = \zeta^{x}_{17,11t2} = 0$. For a molecule with C_{3v} symmetry, such as bicyclopentane-d_1, the corresponding Coriolis interaction is between modes of a_1 and e symmetry and the t_1, t_2 labels must be interchanged. The possible higher order terms $w_{1,1,J}$ and $w_{1,1,k}$ are centrifugal distortion corrections and $w_{1,1,kl}$ is a higher order Coriolis interaction correction.

Since $w_{1,1}$ occurs as an off-diagonal element, its sign cannot be determined in the fitting process but, as discussed by Di Lauro and Mills [10] and Papousek and Aliev [11], with appropriate choice of phase convention, a sign can be given to $w_{1,1}$. We note that, if $w_{1,1}$ is zero and $w_{2,2}$ is the only off-diagonal matrix element, then the fitting process is unable to determine a sign for $w_{2,2}$, but if $w_{1,1}$ is not zero then the sign of $w_{2,2}$ is given by the fitting process, but is independent of the sign of $w_{1,1}$.

An important aid in the rotational assignments for this work was provided by the nuclear spin statistical weights, g_{ns}. For the levels with ro-vibrational symmetry A_1', $g_{ns} = 56$, for those with symmetry A_2', $g_{ns} = 40$, and for those with symmetry E' or E'', $g_{ns} = 80$ [12]. In the ground state those weights result in a 5:5:6:5:5:6... intensity pattern as K increases from $K = 1$, with those levels for which K is divisible by 3 having the weight 6. For $K = 0$ the even J values of the ground state must have A_1 rovibrational symmetry and the odd J values must have A_2 symmetry, thus the 56:40 or 7:5 intensity ratio is helpful in making the J assignments for the $k = 0$ levels. In ν_{18}, the one case where the splitting of the $K = 3$ levels was observed, the intensities showed that for odd J the A_1' level is above the A_2' level, see Fig. 2. By convention then the sign of the splitting parameter Δ_3 is negative.

4. Results and discussion

4.1. The $\nu_{18}(a_2'')$ and $\nu_{13}(e')$ bands of bicyclopentane-d_0

Fig. 2 shows the 800–900 cm^{-1} region containing the $\nu_{18}(a_2'')$ parallel and $\nu_{13}(e')$ perpendicular bands. The mode pictures are from the Gaussian/GaussView output but are somewhat deceptive since they overemphasize the movement of the hydrogens. Normal mode calculations by Wiberg et al. [6] indicate that the ν_{18} mode is best described as 74% skeletal movement of the two axial CH units up and down with respect to the equatorial atoms, with about 20% due to CH_2 wagging motion. For the degenerate ν_{13} mode these calculations indicate about 70% of the mode involves movement of the CH axial units away from the symmetry axis.

The ν_{18} band shows the characteristic P–Q–R shape of a parallel band and the sharp edge of the Q-branch and the regular well-resolved K-structure of each P and R cluster made the J, K assignments of the lines straight-forward. In all, 3182 transitions were assigned, ranging to maximum J and K values of 71 and 60 respectively. These lines were fit using Eq. (2) for upper and lower state levels, with ground state constants set at the values shown in Table 3. These ground state values were determined using the combination-difference method using data from four of the bands studied for bicyclopentane-d_0 (ν_{11}, ν_{14}, ν_{17} and ν_{18}). As discussed in

Table 3
Ground state rotational constants for bicyclopentane-d_0 and bicyclopentane-d_1 (cm^{-1})[a].

	Bicyclopentane-d_0		Bicyclopentane-d_1	
Constant	Experiment	Theory[b]	Experiment	Theory[b]
B_e	–	0.2413	–	0.2280
C_e	–	0.2083	–	0.2083
B_0	0.2399412(2)	0.2387	0.2267506(11)	0.2256
C_0	[0.2058]	0.2058	[0.2058]	0.2058
$D_J \times 10^7$	0.6011(6)	0.609	0.5061(42)	0.513
$D_{JK} \times 10^7$	−0.1833(21)	−0.190	[−0.011]	−0.011
$D_K \times 10^7$	[−0.038]	−0.038	[−0.122]	−0.122
# data	3351		579	
Rms dev.	0.00027		0.00045	

[a] The uncertainties in the last digits (twice the standard deviation) are given in parentheses. Values in brackets were fixed at the theoretical values which for D values are for the equilibrium structure. The number of data is the total number of ground state differences deduced from all bands.
[b] Gaussian 09 B3LYP/cc-pVTZ with Anharm/Vibrot options.

our earlier paper [1], this was done to isolate the ground state parameters from possible errors caused by strong Coriolis interactions in the upper states, especially between ν_{11} and ν_{17}.

We note that the ground state D_J and D_{JK} parameters listed in Table 3 differ very slightly from those given in our previous work [1], where the sextic H constants, which could not be determined from the data analysis, were set to values obtained from the Gaussian calculations. However, subsequently, we have found that the axis orientation chosen automatically by Gaussian in computing the H constants was incorrect. By choosing the correct orientation (using Cartesian input coordinates and the Gaussian Nosymm keyword), we obtain what we believe are the correct theoretical H values. These H parameters are quite small and, since we obtain comparable fits of all data if we fix the H's at these theoretical values or simply set them to zero, the latter is the choice made in obtaining the experimental fits of Table 3.

The fitted upper state values for ν_{18} are given in Table 4. In obtaining these constants, the Coriolis interaction of ν_{18} and ν_{13} was considered. Since the theoretical value of $|w_{1,1}|$, 0.228 cm^{-1}, is small compared to the band separation of about 50 cm^{-1}, the effect of this off-diagonal term can be largely absorbed by compensating changes in the diagonal ΔB contributions of the two states. In Table 4 we report two fits. Fit 1 was made with $w_{1,1}$ set at the theoretical value, 0.228 cm^{-1}, and Fit 2 was made with $w_{1,1}$ set to zero. The quality of fit was excellent in both cases but the average root mean square deviation was very slightly better for Fit 1. Both fits give nearly the same band origin and these are quite close to the theoretical values (within 1%). For ν_{13} ΔC was constrained at the theoretical value but for ν_{18} comparable values were obtained for both fits and the agreement with theory was within 3%. Fit 1 gives a so-called "deperturbed" ΔB^* value while Fit 2 gives a ΔB value which is perturbed since the effect of $w_{1,1}$ is approximately absorbed into the diagonal ΔB contribution to the energy matrix. Conversion between the two values can be done with the Eq. (A2) in Appendix A, where the calculation of these quantities with the Gaussian program is discussed. For ν_{18} the experimental and theoretical ΔB values agree within 5% but this agreement is poorer for the ΔB^* values. However, the latter values are reduced to more reasonable magnitudes and, in all cases the signs agree with those obtained from theory.

At high resolution, the ν_{18} spectra gave clear indication of the Δ_3 splitting of the $K = 3$ levels, as shown in the inset in Fig. 2. This splitting arises from an $h_3(\mathbf{J}_+^6 + \mathbf{J}_-^6)$ term in the Hamiltonian ($h_3 = \Delta_3$) and could be attributed to either the ground or the excited state (or to both). The Gaussian value for h_3 in the ground state is exceedingly small, 2×10^{-15} cm^{-1}, and since the splitting is virtually the same in both the P- and R-branches and since other bands showed no indication of such a splitting for transitions from the $K'' = 3$ ground state levels, we attribute the splitting solely to the upper state of the ν_{18} transition. The value obtained is also quite small, $-0.96(4) \times 10^{-13}$ cm^{-1}, but is of the right magnitude

Table 4
Rovibrational parameters for the ν_{13} and ν_{18} bands of bicyclopentane-d_0 (cm^{-1})[a].

Parameter[b]	$\nu_{13}(e')$			$\nu_{18}(a_2'')$		
	Fit 1	Fit 2	Theory[c]	Fit 1	Fit 2	Theory[c]
w_0			897.6			844.4
ν_0	886.53320(25)	886.5329(4)	873.8	832.92927(3)	832.92900(4)	824.9
$\Delta C \times 10^3$	[−0.234]	[−0.234]	−0.234	−0.2417(8)	−0.25148(12)	−0.259
$\Delta B^* \times 10^3$	−0.5340(22)	*−0.538*	*−0.282*	−0.1584(8)	*−0.144*	*−0.227*
$\Delta B \times 10^3$	*0.435*	0.4320(34)	0.697	*−2.078*	−2.08373(11)	−2.185
$\Delta D_J \times 10^7$	−1.86 (4)	−2.44(8)		−2.34 (4)	−0.726(1)	
$\Delta D_{JK} \times 10^7$	−3.59(20)	−2.85(38)		3.50(4)	2.261(1)	
$\Delta D_K \times 10^7$	2.29(12)	[0]		−1.171(3)	−1.535(2)	
$\Delta H_J \times 10^{11}$	[0]	[0]		−1.53(3)	−0.318(2)	
$\Delta H_{JK} \times 10^{11}$	[0]	[0]		1.72(7)	1.66(1)	
$\Delta H_{KJ} \times 10^{11}$	[0]	[0]		−0.22(5)	−2.43(1)	
$\Delta H_K \times 10^{11}$	[0]	[0]		[0]	1.08(1)	
$\Delta_3 \times 10^{13}$				−0.96(4)	−0.98(6)	
$(C\zeta)_v$	0.09064(10)	0.09006(14)	0.1081			
$\mu_J \times 10^4$	−0.363(9)	−0.381(14)				
$\mu_K \times 10^4$	0.340(14)	[0]				
$q \times 10^3$	*−1.20*	∓1.203(6)	−1.80			
$q^* \times 10^3$	0.725(4)	*±0.74*	*0.154*			
$q_J \times 10^6$	−0.375(8)	±0.491(17)				
$w_{1,1}$	[±0.228]	[0]	0.228			
$w_{1,1J} \times 10^5$	±1.173(20)[d]					
$w_{1,1,kl} \times 10^3$	∓1.17(5)[d]					
# trans.	156	156		3182	3182	
Rms dev.	0.00090	0.00092		0.00014	0.00025	

[a] The uncertainties in the last digits (twice the standard deviation) are given in parentheses.
[b] $\Delta B = B' - B''$, $\Delta C = C' - C''$, etc. Parameter values in brackets were fixed. The theoretical $(C\zeta)_v$ value is $C_v\,\zeta_v$. Deperturbed parameters are labeled with an asterisk. Italicized values were calculated using Eqs. A2,A3, and A6 of Appendix A.
[c] Gaussian 09 B3LYP/cc-pVTZ with Anharm/Vibrot options.
[d] $w_{1,1}$ and $w_{1,1J}$ must have the same sign while $w_{1,1,kl}$ must have the opposite sign.

for this small distortion effect. As indicated in the discussion of the nuclear spin statistics, the splitting constant, Δ_3, is given a negative sign to indicate that for odd J values the A_1' level is above the A_2' level, and vice versa for even J values.

The $\nu_{13}(e')$ perpendicular band proved quite challenging to analyze, in part because the R-branch is significantly obscured by the strong absorptions near 890 cm^{-1} which are believed to be Q-branch transitions of 2-methyl-1-butene. These impurity absorptions are absent in the spectra reported for bicyclopentane-d_0 in Ref. [6] where a value of 886 cm^{-1} is given for ν_{13}. This is consistent with our higher resolution spectra of this region, where the expanded view of Fig. 4 shows a pattern near this position that matches expectations for the $^rQ_0(J)$ branch. In particular 24 lines from 886.1 to 886.3 cm^{-1} show a J-even, J-odd intensity alternation that is in good accord with the predicted nuclear spin weights of 56, 40 respectively. These lines fit nicely the relation $Q_0(J) = Q_0^0 + \Delta B_{eff} J(J+1) - \Delta D_J J^2(J+1)^2$, with Q_0^0, ΔB_{eff}, and ΔD_J equal to 886.568, −0.000205, and -0.19×10^{-8} cm^{-1}, respectively. It is noteworthy that, for $^rQ_0$, the l-doubling constant q has a first-order effect in splitting the $K' = 1$ levels so that $\Delta B_{eff} = \Delta B + \frac{1}{2}q$. The Gaussian calculations predict values of $\Delta B = +0.00070$ cm^{-1} and $q = -0.00180$ cm^{-1} for the upper state of the ν_{13} mode, giving $\Delta B_{eff} = -0.00020$ cm^{-1}, in excellent agreement with the above experimental value. This negative value of ΔB_{eff} is consistent with the red shading observed for the $^rQ_0(J)$ lines with increasing J.

Analysis of other subbands in the spectrum was more difficult. For the other Q branches, $^rQ_1(J)$, $^rQ_2(J)$,…, q is less important and the positive Gaussian value of ΔB predicts that these Q-branch bands should be blue-shaded as J increases, with possible band heads due to the negative and large value of ΔD_J. The J sequences shown in Fig. 4 illustrate this effect, with band heads at $J = 19$ and 27 for the $K = 1$ and 2 Q-branches, respectively. The calculated spectrum shown in Fig. 4 matches nicely the observed spectrum for the low-K Q-branches but the agreement was less impressive for higher-K subbands. Unfortunately, P- and R-branch transitions are low in intensity for low values of K so that the assignments could not be verified. For increasing values of K, it became increasingly difficult to make confident Q-branch assignments and, again, the corresponding P- and R-branch transitions are still low enough in intensity that the Q-assignments could not be verified. In fact, no P- or R-branch transitions for ν_{13} could be assigned due to the spectral complexity and the presence of impurity absorptions. Despite this, it did prove possible to assign 156 Q-lines with reasonable confidence, yielding the ν_{13} parameters shown in Table 4. The resultant ν_{13} values for ν_0, ΔC, $(C\zeta)$, and q are not as reliable as the uncertainties imply but they are in reasonable accord with the theoretical predictions, both in sign and magnitude. The ΔD, ΔH and other higher-order parameters values obtained from the fits are even less certain and should be regarded as tentative.

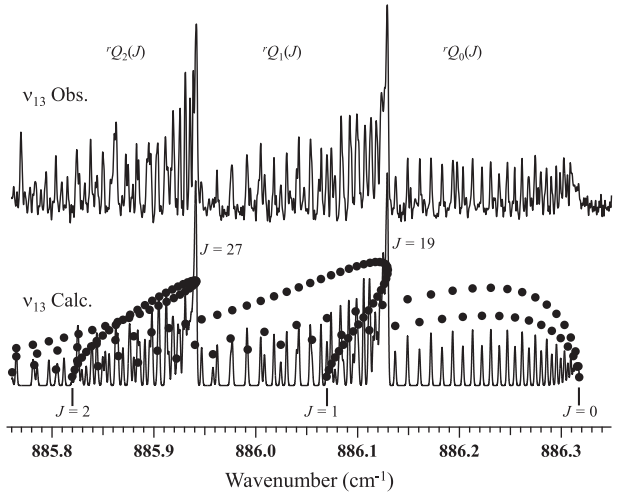

Fig. 4. Expanded view of the ν_{13} Q-branch region of bicyclopentane-d_0. The expected intensity alternation of the J_{odd}, J_{even} lines of the $^rQ_0(J)$ subband is apparent, as is the band heading of the $^rQ_1(J)$ and $^rQ_2(J)$ subbands.

4.2. The $\nu_{17}(a_2'')$ and $\nu_{11}(e')$ bands of bicyclopentane-d_0

Fig. 3 shows the region of the strong ν_{17} band of bicyclopentane-d_0. Although at first glance this has the appearance of a normal parallel band, closer inspection gives clear evidence for a Coriolis interaction with a perpendicular band located slightly above ν_{17}. Our theoretical calculations show that the ν_{11} state should be nearby and slightly higher, and the Coriolis coupling constant, $w_{1,1}$, as given in Eq. (5) should have a value near 0.09 cm^{-1}. The GaussView mode pictures are displayed in Fig. 3 and the normal mode calculations in Ref. [6] indicate that ν_{17} is about 49% skeletal motion (like ν_{18}) and 44% CH_2 wagging motion. ν_{11} is mixed with the off-axis motion of the terminal CH groups but also contains appreciable (28%) bending of the CH units with respect to the symmetry axis.

There are several distinctive features of the ν_{17} band that were helpful in understanding and assigning the spectrum. One feature, visible in Fig. 3, is the sharp rise and fall in the intensities of the P- and R-branch transitions which is due primarily to a reversal in the direction of the shading of the K fine structure. Analogous features were not observed in the 830 cm^{-1} region shown in Fig. 2. The other interesting feature is in the Q-branch region at 1218.6 cm^{-1}. This can be seen in Fig. 3 as a spike that stands out above the other nearby transitions.

These features are related in that they are caused by avoided crossings that affect all three branches at roughly the same J values and that are particularly important at high K for Q-branch transitions and at low K for P- and R-branch transitions. A reduced energy diagram is provided in Fig. 5 that shows that, in the absence of Coriolis interaction, above about $J = 26$ the ν_{17} levels would slice through the $kl > 1$ levels of ν_{11}. Inclusion of this interaction mixes these states and produces the avoided crossing region. To aid in seeing this, the bold traces show levels for the $J = K + 1$ and $J = K + 10$ sequences. The solid line shows states of predominantly ν_{17} character while the dashed lines depict those of mainly ν_{11} character. For the $J = K + 1$ and $J = K + 10$ sequences, the composition of the states switches at about $J = 26$ and 37 respectively.

Fig. 6 shows the region near the $Q_K(28)$ feature at 1218.6 cm^{-1} where the band head is a direct consequence of the avoided crossings. The avoided crossings explain why, at lower J the repulsion causes blue-shading of the K structure of $Q_K(27)$ while at higher J, the shading is to the red for $Q_K(29)$. The mixing of states also affects the intensity of the transitions; the calculated dotted and dashed traces in Fig. 6 shows the intensity if mixing is or is not included, respectively, and the former is clearly favored. Other regions of the Q-branch also reflect the effects of the level crossings, for example there is a feature that looks like a band head at 1220.8 cm^{-1} that is due to the crossing between the levels $J = 27$, $K = 26$ and $J = 29$, $K = 27$ of ν_{11} and $J = 27$, $K = 25$ and $J = 29$, $K = 26$ of ν_{17}. In the case of the P- and R-branches, the more intense lines occur at low K instead of at high K as for the Q-branches. The dominant P- and R- features at 1205.3 and 1231.6 cm^{-1} are ν_{17} transitions that occur to the compressed K levels of $J' = 27$ of the upper state.

The constants resulting from this analysis are given in Table 5. A fairly complete set of 2565 transitions ranging up to $J_{max} = 69$ and $K_{max} = 51$ was measured for the parallel band, ν_{17}. Since transitions of ν_{17} were observed both below and above the perturbed level

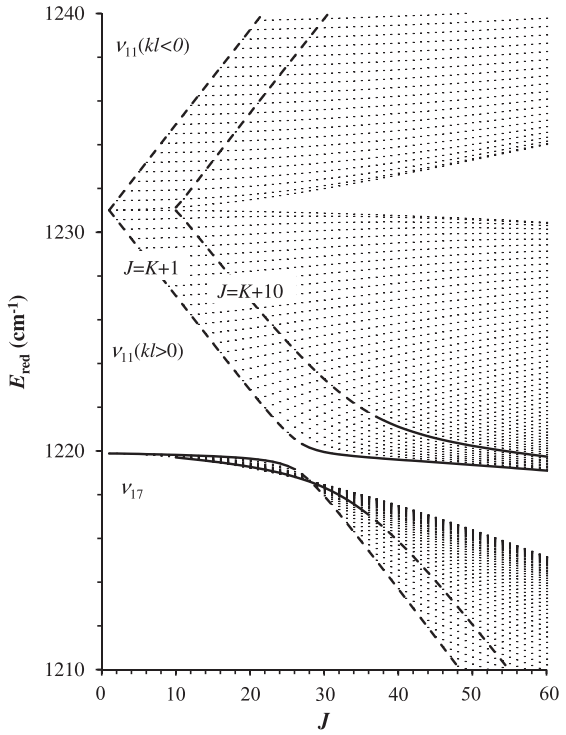

Fig. 5. Avoided crossings in the reduced energy versus J plot of the ν_{11} and ν_{17} upper state levels of bicyclopentane-d_0. $E_{red} = E(J,K',l') - E(J,K,0)$ is equal to the Q-branch wavenumber values for the bands. The $J = K + 1$ and $J = K + 10$ are highlighted to show the trends. The solid (dashed) lines correspond to levels that are predominantly ν_{17} (ν_{11}), with the jumps occurring when the states are nearly equally mixed.

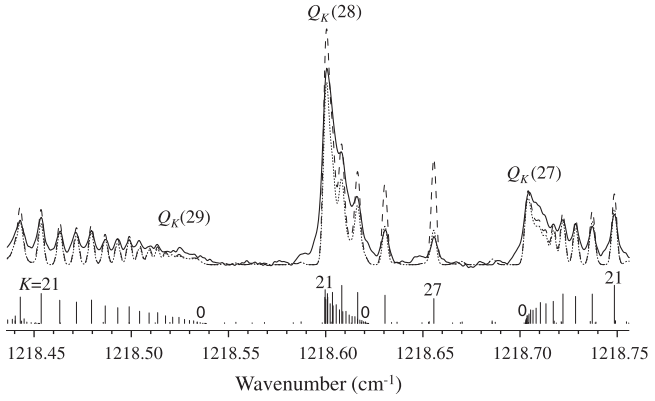

Fig. 6. Expanded view of the ν_{17} Q-branch region of bicyclopentane-d_0. The avoided crossings of Fig. 4 are responsible for the reversal of the shading of the K-structure of the $Q_K(27)$ and $Q_K(29)$ clusters. The dotted and dashed curves correspond to intensities calculated with and without including the effects of mixing, respectively, with the former more closely matching experiment.

crossings with ν_{11}, the analysis is able to give very accurate values for the perturbation constant, $w_{1,1}$.

The 827 transitions found for the ν_{11} band involved primarily those rotational levels that are perturbed and therefore mixed with ν_{17}. Because of the density of the transitions, many of the observed absorption lines were assigned to two different transitions so that, although 827 transitions were in the fit, only about 550 different absorption lines were used for the ν_{11} analysis. Other multiply assigned lines could have been added to the fit but we only accepted lines for which the shape indicated nearly perfect alignment.

Table 5
Rovibrational parameters for the ν_{11} and ν_{17} bands of bicyclopentane-d_0 (cm^{-1})[a].

Parameter[b]	$\nu_{11}(e')$		$\nu_{17}(a_2'')$	
	Experiment	Theory[c]	Experiment	Theory[c]
ω_0		1259.3		1252.3
ν_0	1231.40563(20)	1225.7	1219.88870(5)	1220.7
$\Delta C \times 10^3$	−0.1228(6)	−0.106	−0.2265(2)	−0.219
$\Delta B^* \times 10^3$	−0.2583(2)	−0.164	−0.1160(1)	−0.229
$\Delta B \times 10^3$	*0.504*	*1.090*	*−1.64*	*−2.74*
$\Delta D_J \times 10^8$	0.116(6)		−0.326(4)	
$\Delta D_{JK} \times 10^8$	[0]		0.722(13)	
$\Delta D_K \times 10^8$	−0.445(70)		−0.413(13)	
$(C\zeta)_v$	0.183754(9)	0.186		
$\eta_J \times 10^6$	0.922(6)			
$\eta_K \times 10^6$	−0.964(41)			
$q^* \times 10^3$	0.2175(4)	0.027		
$q \times 10^3$	*−1.306*	*−2.48*		
$w_{1,1}$	±0.093680(2)	0.0937		
$w_{1,1,J} \times 10^6$	∓0.2082(12)[d]			
# trans.	827		2565	
Rms dev.	0.00042		0.00033	

[a] Uncertainties in the last digits (twice the standard deviation) are given in parentheses.
[b] $\Delta B = B' - B''$, $\Delta C = C' - C''$, etc. Parameter values in brackets were held fixed. The theoretical $(C\zeta)_v$ value is $C_v\,\zeta_e$. Deperturbed parameters are labeled with an asterisk. Italicized values were calculated using Eqs. A2,A3, and A6 of Appendix A.
[c] Gaussian 09 B3LYP/cc-pVTZ with Anharm/Vibrot options.
[d] While the sign of $w_{1,1}$ cannot be determined, the sign of $w_{1,1,J}$ must be opposite to the sign of $w_{1,1}$.

The $w_{1,1}$ result agrees extremely well with the predicted value as does the $C\zeta$ value (both within 1%). This is not too surprising since both parameters depend upon Coriolis constants that are accurately obtained at the harmonic level. The anharmonic frequencies, ν_0, predicted for ν_{11} and ν_{17} depend upon cubic and quartic terms in the potential and are both about 3% lower than the harmonic values, ω_0, and are within 0.5% of the experimental values.

The ΔC values include a contribution by the cubic anharmonic terms and theory and experiment agree quite well for ν_{17} (3%) but less well for ν_{11} (14%). In the case of ΔB, the Coriolis coupling of ν_{11} and ν_{17} has a profound effect since the two harmonic frequencies differ by only 7 cm^{-1} and there is a significant resonance contribution, making ΔB about ten times larger than ΔC for ν_{17}. In Appendix A, we discuss this problem briefly and outline the procedures used in Gaussian to obtain more reasonable "deperturbed" ΔB^* values. These have the same sign and magnitude as the "deperturbed" experimental values (i.e. those obtained when the $w_{1,1}$ is included as an off-diagonal term in the fitting process). This appendix also describes how the l-doubling constant q can be obtained from the Gaussian output. As for ΔB, a similarly large reduction in the magnitude of q is obtained when it is "deperturbed". Since the deperturbation of experimental ΔB and q values depends upon the anharmonic frequency difference $\nu_{17}-\nu_{11}$ = 11.5 cm^{-1} while the theoretical deperturbation involves the harmonic difference $\omega_{17}-\omega_{11}$ = 7.0 cm^{-1}, it is not surprising that those experimental values show less good agreement with the theoretical calculations.

4.3. The ν_5 (a_1) and ν_{15}(e) bands of bicyclopentane-d_1

Fig. 7 shows the observed spectrum of our sample of bicyclopentane-d_1 in the region of the strong ν_5 band. Comparison with the spectrum of bicyclopentane-d_0 displayed in Fig. 3 indicates that the -d_1 spectrum is highly contaminated with features due to the -d_0 isotopologue. Fortunately, that contamination does not interfere with the analysis of the strong features of the ν_5 band, but it does make it difficult to find and assign with confidence

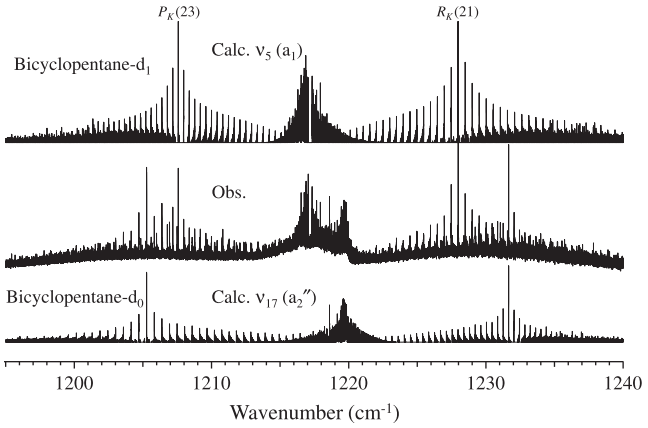

Fig. 7. Overview of the parallel (a_1) ν_5 band region of bicyclopentane-d_1. The sample contains an appreciable amount of the -d_0 isotopologue, as confirmed by the calculated spectra for the parallel bands of both isotopic forms. Not shown is the weak perpendicular (e) ν_{15} band bicyclopentane-d_1 whose band origin is at1210.3 cm^{-1}.

the lines of the much weaker ν_{15} band. The normal mode for ν_5 will be similar to the skeletal motion for ν_{17} of the -d_0 isotopologue and the small 2.6 cm^{-1} isotopic shift on deuteration is consistent with this. For ν_{15}, there is more motion of the axial H atoms and on deuteration, a larger frequency shift of 21 cm^{-1} is observed.

Before the analysis of the ν_5 band was begun, the Gaussian calculations showed that these two vibrational states should be close together and should be coupled with a $w_{1,1}$ term that is close to 0.08 cm^{-1} in value. Since the ν_{15} state is below the ν_5 state, the ν_5 levels do not cross at all for ν_{15} levels with $kl > 0$ but do cross for the $kl < 0$ levels at about $J = 22$, as shown in the reduced energy diagram of Fig. 8. As in the case of bicyclopentane-d_0, the avoided crossing causes a reversal of the fine structure of the P- and R-branch transitions that results in the apparent sharp peak in the intensity of the P-branch transitions at $P(23)$ and in the R-branch transitions at $R(21)$ (see Fig. 7). Note however that the shading of the K structure at low J is to the red, rather than to the blue, as for bicyclopentane-d_0. This is because for the latter, the perturbing band is 11 cm^{-1} above the parallel band, instead of 7 cm^{-1} below as for bicyclopentane-d_1. Since the interacting bands are closer for bicyclopentane-d_1, the reversal also occurs at lower J values, about 22, instead of at about 28 for bicyclopentane-d_0.

The most striking feature of the ν_5 band is the gap in the Q-branch region that is caused by the Coriolis interaction between ν_5 and ν_{15}. That gap is shown in more detail in Fig. 9. From the initial analysis of the P- and R-branch transitions of the parallel ν_5 band, the band center is found to be quite close to 1217.3 cm^{-1}, which agrees with the cluster of lines just above the gap in the Q-branch. The P- and R-branch analysis also shows that the low-K transitions, which are the strongest P- and R-branch transitions, are relatively unperturbed. The strongest Q-branch transitions for a parallel band are those for which $J = K$. The Coriolis interaction has the effect of displacing the low $J = K$ transitions to higher wavenumbers, hence the Q-branch transitions should begin at the band center for ν_5 and go to higher wavenumbers as the value of $J = K$ increases until the crossing point is reached. At this point the Q-branch transitions jump to lower wavenumbers and then, as the separation gets larger, the effect of the Coriolis interaction gets smaller and the Q-branch transitions approach the band center and assume a ΔB value that is more nearly what one would have if the states were not coupled. This behavior can be seen for the highlighted $J = K$ sequence of Fig. 9 in which the jump occurs at 19 and the sequence moves to higher wavenumber until a band head is produced at the $J = K = 26$ transition near 1217.052 cm^{-1}.

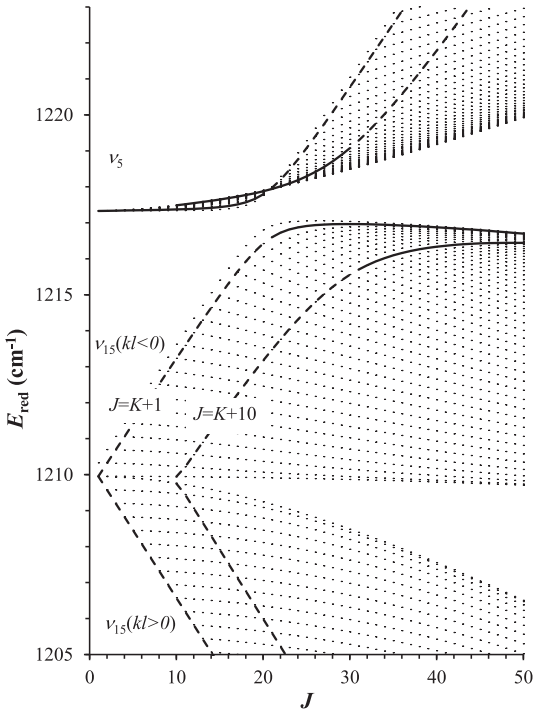

Fig. 8. Avoided crossings in the reduced energy versus J plot of the ν_5 and ν_{15} upper state levels of bicyclopentane-d_1. $E_{red} = E(J,K',l') - E(J,K,0)$ is equal to the Q-branch wavenumber values for the bands. The $J = K + 1$ and $J = K + 10$ are highlighted to show the trends. The solid (dashed) lines correspond to levels that are predominantly ν_5 (ν_{15}), with the jumps occurring when the states are nearly equally mixed.

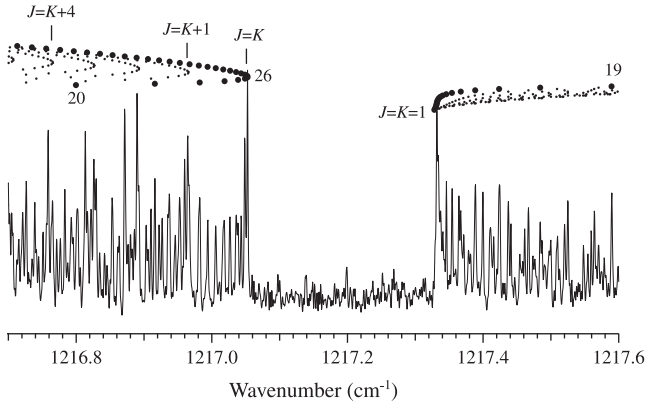

Fig. 9. Expanded view of the ν_5 Q-branch region of bicyclopentane-d_1. The avoided crossings of Fig. 7 are responsible for the gap in this region and produce the band heads of the $J = K + n$ sequences. This band head occurs at 26 for the highlighted $J = K$ sequence, which also shows the avoided crossing jump as J goes from 19 to 20.

Each value of n, where $J = K + n$, results in a different band head so that for $n = 1$, $J = 30$, $K = 29$ is at the band head at 1216.965 cm^{-1}, and for n = 2, $J = 33$, $K = 31$ is at the band head at 1216.893 cm^{-1} and so on with other band heads at 1216.83 and at 1216.77 cm^{-1}.

As a general rule it is difficult to determine the effects of a Coriolis interaction if there is no level crossing and/or if only transitions are observed for levels below (or above) any crossing point. As in the -d_0 case, however, many (1517) transitions to rotational levels of ν_5 both above and below the crossing are observed so the $w_{1,1}$ constant is well-determined. We have also been able to identify 118 transitions that are primarily ν_{15} although they contain a significant amount of mixing with ν_5.

Table 6
Rovibrational parameters for the ν_5 and ν_{15} bands of bicyclopentane-d_1 (cm^{-1})[a].

Parameter[b]	$\nu_{15}(e')$		$\nu_5(a_1)$	
	Experiment	Theory[c]	Experiment	Theory[c]
ω_0		1238.0		1249.7
ν_0	1210.30664(47)	1205.6	1217.32680(6)	1217.5
$\Delta C \times 10^3$	−0.1681(20)	0.056	−0.22411(23)	−0.214
$\Delta B^* \times 10^3$	−0.1911(6)	*−0.121*	−0.0561(2)	*−0.115*
$\Delta B \times 10^3$	*−1.006*	−0.661	*1.573*	0.966
$\Delta D_J \times 10^8$	[0]		−0.142(8)	
$\Delta D_{JK} \times 10^8$	[0]		0.549(26)	
$\Delta D_K \times 10^8$	[0]		−0.405(22)	
$(C\zeta)_v$	0.167562(19)	0.162		
$\eta_J \times 10^6$	0.144(30)			
$q^* \times 10^3$	0.1856(9)	*0.066*		
$q \times 10^3$	*1.815*	1.147		
w_{11}	±0.075627(3)	0.0795		
# trans.	118		1517	
Rms dev.	0.00044		0.00039	

[a] Uncertainties in the last digits (twice the standard deviation) are given in parentheses.
[b] $\Delta B = B' - B''$, $\Delta C = C' - C''$, etc. Parameter values in brackets were held fixed. The theoretical $(C\zeta)_v$ value is $C_v\,\zeta_v$. Deperturbed parameters are labeled with an asterisk. Italicized values were calculated using Eqs. A2,A3, and A6 of Appendix A.
[c] Gaussian 09 B3LYP/cc-pVTZ with Anharm/Vibrot options.

In fitting these transitions, in order to ensure that the ground state constants are not affected by an imperfect accounting for the effects of the Coriolis interaction between ν_5 and ν_{15}, we have fit the ground state combination-differences to determine the values of B_0 and D_J given in Table 3. The combination-differences did not include a wide enough range of values for K to determine D_{JK} so the theoretical value was used in all the fits, as was also the case for C_0 and D_K.

These ground state constants were then held fixed in fitting the larger data set to determine the upper state parameters presented in Table 6 for the ν_5 and ν_{15} modes.

The comparison of theoretical and experimental values in Table 6 shows good agreement for the anharmonic frequencies and for $w_{1,1}$ and $C\zeta$. The values of ΔC are quite similar for the parallel ν_5 case but are in poor agreement and differ in sign for the less well characterized ν_{15} mode. As for bicyclopentane-d_0, a resonance correction to the experimental values is necessary to obtain "deperturbed" values of ΔB^* and q^*. It is interesting that the Gaussian program uses a default upper limit of 10 cm^{-1} for the difference in the harmonic frequencies in determining whether or not to exclude the Coriolis resonant term in calculating ΔB. For bicyclopentane-d_0, this difference $\omega_{17}-\omega_{11} = -7.0$ cm^{-1} and the results give "deperturbed" values ΔB^* and q^*. For bicyclopentane-d_1, the difference $\omega_5-\omega_{15} = +11.7$ cm^{-1} and the Gaussian results are perturbed ΔB and q values. Conversion between perturbed and "deperturbed" values are made using Eqs. A2,A3, and A6 in Appendix A and values calculated in this manner are indicated with italics in Tables 4–6.

4.4. Ground state properties

Table 3 lists the ground state rotational parameters determined for both isotopologues of bicyclopentane. In both cases, B_0 is very well determined and is about 0.5% larger than the theoretical result. For bicyclopentane-d_0, our value 0.2399412(2) cm^{-1} falls slightly outside the uncertainty estimates of Wiberg et al. [6] in their determination of a value of 0.23961(7) cm^{-1}. This discrepancy is not too surprising since the latter studies were done at much lower resolution (0.06 cm^{-1}) where the K structure of the P and R lines could not be resolved. These authors did not report B_0 for the -d_1 isotopologue but, at the same resolution, they did obtain a value of 0.21440(5) cm^{-1} when both axial hydrogens were replaced by deuterium atoms (-d_2).

Wiberg's data did not allow a determination of centrifugal distortion effects but our higher resolution data do. The D_J values obtained agree nicely with theory, with values for the -d_0 and -d_1 species only 1.4% smaller than the theoretical values. Although D_{JK} could not be determined for the -d_1 isotopologue, the value for bicyclopentane-d_0 is within 4% of the predicted value. The good agreement between theory and experiment seen here, and also for many upper state parameters shown in Tables 4–6, mirrors what we have seen for other small molecules. These results demonstrate that Gaussian calculations at the anharmonic level using the B3LYP method with a cc-pVTZ basis can be quite accurate and a useful aid in unraveling often complex molecular spectra.

In Table 7, we compare structural parameters determined for bicyclopentane with theoretical values calculated in this study. Electron diffraction experiments [13] give the basic structure of the molecule in terms of thermally-averaged parameters (R_a), while the theoretical calculations give an equilibrium structure (R_e) for the particular method/basis chosen. When done at the anharmonic level, the calculations also give a thermally averaged structure (R_z) at 0 K. Small but important differences exist between these various structures, as discussed in detail in the literature [14–16]. In general, it is found that the order of bond lengths is $R_e < R_z < R_a$ and such is the case for all direct bonds in

Table 7
Experimental and theoretical structural parameters for bicyclopentane-d_0 and -d_1.

Parameter	Unit	Elec. Diff.[a]	Theory[b]		
		(R_a)	(R_e)	(R_z)-d_0	(R_z)-d_1
$R_{eq} = C_{ax}–C_{eq}$	Å	1.557(2)	1.5542	1.5629	1.5628
$R_{ax} = C_{ax}–C_{ax}$	Å	1.874(4)	1.8764	1.8855	1.8854
$r_{eq} = C_{eq}–H$	Å	1.107(4)	1.0902	1.0971	1.0971
$r_{ax} = C_{ax}–H$	Å	1.107(4)	1.0885	1.0953	1.0952
$r'_{ax} = C_{ax}–D$	Å				1.0938
β = H–C–H	deg.	111.7(18)	111.559	111.393	111.390
I_C	amu-Å2	81.77	80.935	81.896	81.887
C	cm^{-1}	0.2062	0.20828	0.20572	0.20574
C_0	cm^{-1}			0.20584	0.20586
I_B	amu-Å^2	70.38	69.8729	70.6270	74.7209
B	cm^{-1}	0.2395	0.24130	0.23851	0.22544
B_0	cm^{-1}			0.23870	0.22561
B_0 (Exp.)	cm^{-1}			0.2399412(2)	0.2267506(11)
I_{Bo}	amu-Å^2			70.25734(6)	74.34437(36)

(R_e) refers to the equilibrium structure. (R_z) refers to a vibrationally-averaged structure at 0 K.
[a] Thermal-average (R_a) parameters (Ref. [13]). The uncertainties in the last digits are in parentheses.
[b] This work, using Gaussian 09 (B3LYP/cc-pVTZb with Anharm/Vibrot options).

bicyclopentane. However, for the non-bonded C_{ax}–C_{ax} distance, the electron diffraction value is noticeably lower than the calculated R_e and R_z values. It is difficult to assess the significance of this since the diffraction data also could not distinguish separate axial and equatorial CH distances nor could they eliminate the possibility of a CH_2 twist of up to 11° out of the equatorial plane to yield a structure of D_3 symmetry. The latter seems unlikely however and the theoretical calculations clearly show a minimum for the D_{3h} structure so this is assumed in the calculations below.

The moments of inertia are related to the five structural parameters of bicyclopentane by the equations [6]

$$I_z = 3M_C a^2 + 6M_H[(a + r_{eq}\sin\beta/2)^2 + (r_{eq}\cos\beta/2)^2], \quad (7)$$

$$\begin{aligned} I_x = I_y &= 2M_C[(R_{ax}/2)^2 + (a\sin 60)^2] \\ &+ 2M_H[a\sin 60 + r_{eq}\cos(\beta/2 - 30)]^2 \\ &+ 2M_H[a\sin 60 + r_{eq}\sin(60 - \beta/2)]^2 \\ &+ 2M_H(r_{eq}\sin\beta/2)^2 + 2M_H(r_{ax} + R_{ax}/2)^2, \end{aligned} \quad (8)$$

where $a = [R_{eq}^2 - (R_{ax}/2)^2]^{1/2}$ is the distance of the equatorial carbon to the center of mass and the other parameters are defined in Table 7. These equations apply for the equilibrium structure but it is common to use them also in extracting information from B and C values given by spectroscopic measurements.

The moment about the principal axis $I_z = I_C$ is unaffected by isotopic substitution for any of the atoms on the C_3 axis and hence the C_e rotational constant will be identical for the -d_0 and -d_1 isotopologues studied here. The normally allowed infrared transitions are unable to determine a value for C_0 but under certain circumstances, such as for some Coriolis interactions, it is possible to use infrared data to determine a value for C_0 [17]. That was not possible in the present case.

However the analyses do give two accurate B_0 and I_{B0} values and these place constraints on the structural parameters of bicyclopentane. Since the substitution is of a single D for an H on the symmetry axis, it can be shown [14,18,19] that the z coordinate of the D atom relative to the center of mass of the -d_0 molecule is given directly by

$$z(D) = \{[I_{B0}(D) - I_{B0}(H)](M + \Delta m)/(M\Delta m)\}^{1/2}, \quad (9)$$

where M is the mass of bicyclopentane-d_0 and Δm is the D–H mass difference. This equation takes into account the shift of center of mass for this mono substitution and, using this equation and the I_{B0} values of Table 7, we calculate $z = (r_{ax} + R_{ax}/2) = 2.0302(2)$ Å. We note that if both axial hydrogens are replaced by deuterium, the center of mass is not shifted and only the last term of Eq. (8) is changed. Using the -d_0 and -d_2 results of Wiberg with Eq. (8) yields a value of 2.027(7) Å for z, which is in good agreement with our more accurate value. It should be noted that specific values of r_{ax} and R_{ax} cannot be determined from the B_0 values, even if determined for all three isotopologues. Also, the use of Eqs. (8) and (9) assumes that none of the structural parameters change on isotopic substitution, an assumption supported by the nearly identical theoretical R_z parameters in Table 7. The exception to this is a small decrease of 0.0015 Å for the axial CD bond length compared to that for CH. A comparable decrease of about 0.002 Å has been observed in other hydrocarbons and is often applied in structural determinations [14,20]. If we assume a decrease of 0.0015 Å, the use of Eq. (12) gives a value of 2.0309(2) Å for $(r_{ax} + R_{ax}/2)$ in bicyclopentane-d_0. This so-called R_s substitution value is somewhat smaller than respective values of 2.044(6), 2.0267 and 2.0381 for the R_a, R_e and R_z structures of Table 7. In general, R_s bond length values are expected to be closest to R_e values and to be less than R_a and R_z values [14], as observed.

To go further in calculating other structural parameters would require additional assumptions and/or experimental values of C_0 as well as corrections of the parameters to a common basis such as R_z or R_s. However, even in the absence of such added information, we believe it can be said that, to a high degree, the current electron diffraction, spectroscopic, and theoretical results are all in very good accord.

Acknowledgments

J. Nibler acknowledges the support of the Camille and Henry Dreyfus Foundation in the form of a Senior Scientist Mentor Award. The research described here was performed, in part, in the Environmental Molecular Sciences Laboratory, a national scientific user facility sponsored by the Department of Energy's Office of Biological and Environmental Research and located at Pacific Northwest National Laboratory (PNNL). PNNL is operated for the United States Department of Energy by the Battelle Memorial Institute under contract DE-AC05-76RLO 1830. We thank Robert Sams of PNNL for advice and assistance in recording the infrared spectra of bicyclopentane in this facility and Gaussian, Inc. for helpful responses to several queries about the use of Gaussian 09 for anharmonic calculations.

Appendix A. Extraction of symmetric top α and q values from Gaussian output

As discussed by Barone [21], the Gaussian calculations of vibration–rotation α constants are based on Eq. (A1)

$$\begin{aligned} -\alpha_r^x = &\frac{2(B^{(x)^2})}{\omega_r}\sum_{\xi}\frac{3(a_r^{(x\xi)^2})}{4I_\xi} + \frac{2(B^{(x)^2})}{\omega_r}\sum_s(\zeta_{r,s}^{(x)})^2\frac{3\omega_r^2+\omega_s^2}{\omega_r^2-\omega_s^2} \\ &+ \frac{2(B^{(x)^2})}{\omega_r}\pi\left(\frac{c}{h}\right)^{1/2}\sum_s\varphi_{rrs}a_s^{(xx)}\frac{\omega_r}{\omega_s^{3/2}}, \end{aligned} \quad (A1)$$

which is applicable to nondegenerate modes of asymmetric tops. The first term comes from the moment of inertia derivatives (a_r) for mode r, the second from the $\zeta_{r,s}$ Coriolis interactions of modes r and s, and the last term gives the contribution of the cubic anharmonic terms φ_{rrs}. We note that the first two terms can be calculated from harmonic quadratic potential constants while the last term involves only cubic and no quartic constants. It can be seen that the Coriolis term becomes quite large when ω_r is near ω_s and the Gaussian program appears to deal with this by eliminating contributions for which $|\omega_r - \omega_s| < 10\ \mathrm{cm}^{-1}$. This serves to eliminate the resonance problem for degenerate modes (t_1, t_2) and α_t for the pair of modes is obtained simply as $\alpha_t = 1/2(\alpha_{t1}^x + \alpha_{t1}^y)$, where t_1 is the index of the mode that is symmetric to a reflection in a symmetry plane containing the primary z symmetry axis. (The t_2 component is antisymmetric to this reflection. Here and below, the alpha value refers to the vibration–rotation correction to the B rotational constant.)

It often happens that two modes that are not degenerate are within 10 cm^{-1} of each other and can Coriolis-interact. The most common case is when a nondegenerate mode (s) interacts with a degenerate mode (t) via an x–y Coriolis coupling; an example occurs in bicyclopentane-d_0 for the $\nu_{17}(a_2'')$ and $\nu_{11}(e')$ modes for which the harmonic frequencies are 1252.3 and 1259.3 cm^{-1}, respectively. In this case, the incorporation of the corresponding resonant term in the diagonal α energy term is not justified and the effect of the resonance is more accurately accounted for by the off-diagonal term $w_{1,1}$ of Eq. (6). The vibration-rotation coupling constant in this case is said to be "deperturbed" and is given the symbol α^*. Unfortunately, the Gaussian output does not distinguish α^* from α values and the user must check for the resonance condition in comparing theoretical and experimental parameters.

To a good approximation, the resonant Coriolis term reduces to 4 $(B\zeta^{y}_{s,t1})^2/(\omega_s-\omega_t)$ and the constants can be related by the relations

$$\alpha_s \sim \alpha^*_s - 4(B_e\zeta^{y}_{s,t1})^2/(\omega_s-\omega_t) \sim \alpha^*_s - 2w^2_{1,1}/(\omega_s-\omega_t) \text{ and,} \quad \text{(A2)}$$

$$\alpha_t \sim \alpha^*_t + 2(B_e\zeta^{y}_{s,t1})^2/(\omega_s-\omega_t) \sim \alpha^*_t + w^2_{1,1}/(\omega_s-\omega_t). \quad \text{(A3)}$$

We have used these relations and definitions such as $B'_s - B''_s = \Delta B_s = -\alpha_s$ in interconverting theoretical ΔB_s, ΔB^*_s and ΔB_t, ΔB^*_t pairs that are listed in Tables 4–6. Similar conversions were made of experimental ΔB pairs but with use of the experimental $w_{1,1}$ parameter and with observed frequencies ν replacing the ω values.

Although not given directly, the Gaussian output can also be used to deduce the symmetric top l-doubling constant q given in Eq. (6). The theoretical expression for this constant is given by Mills [22] and contains terms similar to those in Eq. (A1).

$$-q_t = \frac{2B^2}{\omega_t}\frac{3(\alpha^{(xz)^2}_{t1})}{4I_A} + \frac{2B^2}{\omega_t}\sum_s[(\xi^{(x)}_{s,t1})^2 - (\xi^{(y)}_{s,t1})^2]\frac{3\omega_t^2+\omega_s^2}{\omega_t^2-\omega_s^2} + \frac{2B^2}{\omega_t}\pi\left(\frac{c}{h}\right)^{1/2}\sum_{t'}\varphi'_{t1t1t1'}[a^{(xx)}_{t1'} - a^{(yy)}_{t1'}]\frac{\omega_t}{\omega^{3/2}_{t'}}. \quad \text{(A4)}$$

Taking into account the symmetry properties of α, ζ, and φ for a symmetric top, we have confirmed from the equations and from explicit calculations using the Gaussian output that

$$q = q_{t1} = \alpha^x_{t1} - \alpha^y_{t1}, \quad \text{(A5)}$$

where t_1 refers to the symmetric component of the degenerate mode. (This mode can be identified by examination of the normal modes such as those shown in Figs. 2 and 4 or, more simply, by confirming that a nonzero value exists for φ_{t1t1t1} and not for φ_{t2t2t2}.) The same Coriolis resonance problem occurs for q as for α and both q and "deperturbed" q^* values obtained from the relation

$$q_t \sim q^*_t + 4(B\zeta^{y}_{s,t1})^2/(\omega_s-\omega_t) \sim q^*_t + 2w^2_{1,1}/(\omega_s-\omega_t), \quad \text{(A6)}$$

are listed in Tables 4–6.

Appendix B. Supplementary material

Supplementary data for this article are available on ScienceDirect www.sciencedirect.com) and as part of the Ohio State University Molecular Spectroscopy Archives (http://msa.lib.ohio-state.edu/jmsa_hp.htm).

Supplementary data associated with this article can be found, in the online version, at http://dx.doi.org/10.1016/j.jms.2012.06.008.

References

[1] M.A. Martin, A. Perry, T. Masiello, K. Schwartz, J.W. Nibler, A. Weber, A. Maki, T.A. Blake, J. Mol. Spectrosc. 262 (2010) 42–48.
[2] R. Kirkpatrick, N. Yariyasopit, A. Weber, J.W. Nibler, A. Maki, T.A. Blake, Th. Hubler, J. Mol. Spectrosc. 248 (2008) 153–160.
[3] R. Kirkpatrick, T. Masiello, N. Yariyasopit, J.W. Nibler, A. Maki, T.A. Blake, A. Weber, J. Mol. Spectrosc. 253 (2009) 41–50.
[4] A. Maki, A. Weber, J.W. Nibler, T. Masiello, T.A. Blake, R. Kirkpatrick, J. Mol. Spectrosc. 264 (2010) 26–36.
[5] K.B. Wiberg, Found. Chem. 6 (2004) 65–80.
[6] K.B. Wiberg, R.F. Rosenberg, S.T. Waddell, J. Phys. Chem 96 (1992) 8293–8303. and references to earlier papers contained therein.
[7] Gaussian 09, Revision B.01, M.J. Frisch, G.W. Trucks, H.B. Schlegel, G.E. Scuseria, M.A. Robb, J.R. Cheeseman, G. Scalmani, V. Barone, B. Mennucci, G.A. Petersson, H. Nakatsuji, M. Caricato, X. Li, H.P. Hratchian, A.F. Izmaylov, J. Bloino, G. Zheng, J.L. Sonnenberg, M. Hada, M. Ehara, K. Toyota, R. Fukuda, J. Hasegawa, M. Ishida, T. Nakajima, Y. Honda, O. Kitao, H. Nakai, T. Vreven, J.A. Montgomery, Jr., J.E. Peralta, F. Ogliaro, M. Bearpark, J.J. Heyd, E. Brothers, K.N. Kudin, V.N. Staroverov, T. Keith, R. Kobayashi, J. Normand, K. Raghavachari, A. Rendell, J.C. Burant, S.S. Iyengar, J. Tomasi, M. Cossi, N. Rega, J.M. Millam, M. Klene, J.E. Knox, J.B. Cross, V. Bakken, C. Adamo, J. Jaramillo, R. Gomperts, R.E. Stratmann, O. Yazyev, A.J. Austin, R. Cammi, C. Pomelli, J.W. Ochterski, R.L. Martin, K. Morokuma, V.G. Zakrzewski, G.A. Voth, P. Salvador, J.J. Dannenberg, S. Dapprich, A.D. Daniels, O. Farkas, J.B. Foresman, J.V. Ortiz, J. Cioslowski, D.J. Fox, Gaussian, Inc., Wallingford CT, 2010.
[8] K.R. Mondanaro, W.P. Dailey, Org. Synth. 75 (1998) 98.
[9] A.G. Maki, J.S. Wells, Wavenumber Calibration Tables from Heterodyne Frequency Measurements, NIST Special Publication 821, U.S. Department of Commerce, 1991. <http://physics.nist.gov/PhysRefData/wavnum/html/contents.html> (updated 1995).
[10] C. Di Lauro, I.M. Mills, J. Mol. Spectrosc. 21 (1966) 386–413.
[11] D. Papousek, M.R. Aliev, Molecular Vibrational–Rotational Spectroscopy, Elsevier, Amsterdam/New York, 1982.
[12] A. Weber, J. Chem. Phys. 73 (1980) 3952–3972.
[13] A. Almenningen, B. Andersen, B.A. Nyhus, Acta Chem. Scand. 25 (1971) 1217–1223.
[14] A.G. Robiette, The interplay between spectroscopy and electron diffraction, in: Molecular Structure by Diffraction Methods, The Chemical Society, London, 1973, pp. 160–197 (Chapter 4).
[15] T. Oka, J. Phys. Soc. Jpn. 15 (1960) 2274–2279.
[16] K. Kuchitsu, T. Fukuyama, Y. Morino, J. Mol. Struct. 4 (1969) 41–50.
[17] A.G. Maki, T. Masiello, T.A. Blake, J.W. Nibler, A. Weber, J. Mol. Spectrosc. 255 (2009) 56–62.
[18] C.C. Costain, J. Chem. Phys. 29 (1958) 864.
[19] W.C. Gordy, R.L. Cook, Microwave Molecular Spectra, 3rd ed., Knovel, 1984.
[20] J.L. Duncan, D.C. McKean, A.J. Bruce, J. Mol. Spectrosc. 74 (1979) 361–374.
[21] V. Barone, J. Chem. Phys 122 (2005) 014108-1–014108-10.
[22] I. Mills, Vibration-rotation structure in asymmetric- and symmetric-top molecules, in: Molecular Spectroscopy: Modern Research, Academic Press, New York, 1972, pp. 115–140.